Integrated Process for Structuring and Functionalizing Ordered Mesoporous Silica to Achieve Superprotonic Conductivity

Jason Richard, Anthony Phimphachanh, Julien Schneider, Shyamapada Nandi, Eline Laurent, Patrick Lacroix-Desmazes, Philippe Trens, Sabine Devautour-Vinot, Nathalie Marcotte, Corine Gérardin

An integrated process for structuring and functionalizing ordered mesoporous silica to achieve superprotonic conductivity

Jason Richard,[1] Anthony Phimphachanh,[1,2] Julien Schneider,[1] Shyamapada Nandi,[1] Eline Laurent,[1] Patrick Lacroix-Desmazes,[1] Philippe Trens,[1] Sabine Devautour-Vinot,[1] Nathalie Marcotte[1] and Corine Gérardin[1]*

[1] *Institut Charles Gerhardt, Pôle Chimie Balard Recherche, 1919 route de Mende, 34293 Montpellier cedex 5, France*

[2] *Laboratoire Charles Coulomb, Université Montpellier, Place Eugène Bataillon, CC069F, 34095 Montpellier cedex 5, France*

* email: corine.gerardin@enscm.fr

Abstract

Polyacid-functionalized inorganic mesoporous materials have attracted considerable interest as catalysts, permselective molecular sieves or drug carriers. Despite their great interest, their synthesis into ordered mesostructures incorporating polyacids densely and homogeneously distributed in the mesopores, is a challenge. Moreover, their properties as conductors for energy applications remain completely unexplored. Here we report an efficient, one-shot environmentally friendly synthesis route to prepare ordered mesoporous silica functionalized with strong polyacids, which exhibits excellent proton conductivity. We used polyion electrostatic complex micelles as structure-directing, functionalizing and pore-generating agents to obtain a material of remarkable textural and functional quality. It presents large and ordered mesopores hosting monodisperse polyacid chains corresponding to a dense and homogeneous functionalization of 1.2 $mmol_{SO_3H}.g_{SiO_2}^{-1}$ and a function density of 1 SO_3H per nm^3 of mesopore volume. Overcoming the performance-limiting inhomogeneities, we designed a superprotonic conductor, while the high value of the conductivity, 0.024 S cm^{-1} at 363 K/95% relative humidity, was maintained at least 7 days.

Introduction

Ordered mesoporous silica (OMS) functionalized by polymers is an emerging class of hybrid materials that combines the singular textural characteristics of inorganic networks with the

specific physico-chemical properties of polymers. This gives the materials unique properties that can be attractively triggered by environmental *stimuli*.[1–3] Among OMS, those functionalized with polyacids have proven to be particularly attractive for their acidic properties, complexation ability and pH-responsiveness, showing excellent performances in many applications such as heterogeneous catalysts,[4–8] permselective mesoporous thin films[9,10] and drug carriers,[11–13] to name a few. Surprisingly, the proton conduction performance of OMS functionalized with strong polyacids has never been reported, despite the discovery of promising porous materials as proton conductors, *e.g.* porous sulfonated organic polymers[14] and *mono*sulfonated OMS.[15–19] Obviously, the substitution of a *mono*sulfonic acid function with a *poly*sulfonic acid in the porous framework of a stable inorganic backbone is expected to increase the number of labile protons, resulting in a higher density of acid functions for a similar mesopore size. Therefore, the already promising proton conductivity (7.2 x 10^{-3} $S.cm^{-1}$) observed by Mikhailenko et al.[15] for *mono*sulfonic acid-functionalized OMS particles should be improved.

The lack of studies on materials functionalized with polysulfonic acids is due to the difficulty in achieving dense and homogeneous functionalization of the mesoporous silica as well as controlled polymer characteristics, including dispersity and block molecular weights. Most current polymer functionalization strategies rely on post-functionalization of mesopores using the "grafting to"[11] or "grafting from"[4,5] approaches. In these respective approaches, a polymer is either grafted onto the pore surface or grown by *in situ* polymerization from the activated surface. While the "grafting to" method results in inhomogeneous functionalization with presynthesized polymers of controlled molecular weight, the "grafting from" method produces polymers of polydisperse molecular weight, which can ultimately be densely integrated, but at the expense of the pore volume required for most of applications.[20] Furthermore, regardless of the post-functionalization strategy, an ordered porous material must first be synthesized. This requires numerous steps involving the use of many solvents and reagents, high energy consumption to remove the pore-forming sacrificial agent directing the silica structure, which subsequently limits the large-scale development of such polymer-functionalized OMS. Alternatively, one-pot synthesis strategies for functionalizing OMS with polyacids should be suitable methods to overcome those limitations, using a pre-synthesized polyacid directly introduced into the synthesis medium. In this context, perfluorobutylsulfonylimide-based alkoxysilanes were co-condensed with tetraethoxysilane (TEOS) under sol–gel conditions.[21] However, non-uniform agglomerated mesoporous particles with irregular porosity were obtained. Even the presence of a structure-directing agent in the synthesis medium did not improve the formation of an ordered silica mesophase. As reported, [22] silica nanoparticle agglomerates without structure or with missing porosity were obtained

by mixing quaternary ammonium surfactants with perfluorosulfonic acid ionomers and TEOS. These examples highlight the difficulty of precisely controlling the interactions between all the reactants in a one-pot synthesis, which is crucial for obtaining polyacid functionalized OMS with controlled structure and specific functionalities. Given these limitations, it is imperative to design new routes for direct functionalization of OMS with polyacids to improve the quality and efficiency of functionalization. This includes controlling the length, dispersity and spatial distribution of polymers, combined with reducing the environmental impact of the synthesis method.

In this work, we present a method for the direct and environmentally friendly functionalization of ordered mesoporous silica with strong polyacids of perfectly defined length, which are densely and homogeneously distributed in the mesopores. The strategy relies on the use of a novel structure-directing agent, namely polyion complex (PIC) assemblies, which incorporate desired functionalities that are masked during the sol–gel process, preventing disruption of the mesostructuring process. As reported,[23–26] PIC micelles formed with a weak polyacid-based double-hydrophilic block copolymer (DHBC) and an oppositely charged polyelectrolyte direct the structure of PIC-silica materials with tunable textural and structural properties (2D hexagonal, lamellar, cubic), called MesoPIC materials. In most subsequent studies, the PIC assembly has been completely removed from the organic-inorganic hybrid material. In the present study, we seek to preserve the DHBC of the PIC assembly in the material to give acidic properties to the pores, using a strong polyacid-based DHBC containing a poly(styrene sulfonic acid) (PSS) block. The new PSS-functionalized OMS is hereafter referred to as MesoPIC-PSS. The process operates under purely aqueous conditions and at room temperature, making it an environmentally friendly and energy-efficient synthesis procedure. The resulting MesoPIC-PSS material obtained has a very high volume density of 1 SO_3H function per nm^3 of mesopore volume; it also exhibits a superprotonic conductivity, i.e. $\sigma = 2.4 \times 10^{-2}$ $S.cm^{-1}$ at 363 K / 95 % Relative Humidity (RH), as well as constant performances maintained for 7 days, proving its excellent hydrolytic and chemical stability. These results demonstrate for the first time the interest of mesoporous silica functionalized with polyacids as proton conductors.

Experimental Section

Chemicals

Oligochitosan with a molar mass of 2500 g.mol^{-1} was purchased from Creative PegWorks® and used as received. A deacetylation degree of 97% was measured by ^{1}H NMR. The following global molar composition was determined by a combination of ^{1}H NMR analysis, TGA, elemental analysis, aqueous acid-base titration, conductivity and chloride concentration measurements: DeacetylatedUnit(0,97), AcetylatedUnit(0,03), $C_3H_5O_3$(0,52), Cl^-(0,48), H_2O(0,85), where $C_3H_5O_3$ is lactate counter-ion. A small amount of inorganic cations may be present but was not detected. Tetraethoxysilane (TEOS), 2-(Dodecylthiocarbonothioylthio)-2-methylpropionic acid (DDMAT, 98%), sodium 4-vinylbenzenesulfonate (SSNa, ≥ 90% technical grade), 4,4'-Azobiscyanopentanoic acid (ACPA, Aldrich, 98%) were purchased from Sigma-Aldrich and used as received. Poly(ethylene glycol) methyl ether acrylate (APEO, M_n =480 g.mol^{-1}, 8.5 EO units on average) was purchased from Sigma-Aldrich; prior to use, APEO was stirred for 30 minutes with basic alumina and filtered to remove the inhibitor. The chemical formula of DDMAT, APEO, and SSNa are represented in Figure S1.

Synthesis of PAPEO-*b*-PSS

Synthesis of Poly(poly(ethylene glycol)-methyl ether acrylate) by aqueous RAFT Polymerization of APEO

Synthesis of P(APEO)$_{25}$-DDMAT was adapted from a previous work[27] and performed as follows: DDMAT (0.55 g, 1.5 mmol, 1 eq), APEO (15 g, 31.3 mmol, 20.9 eq), ACPA (0.08 g, 0.3 mmol, 0.2 eq) and distilled water (12.79 g) were introduced in a round-bottom flask and stirred (solids content= 55 %). The mixture was degassed with nitrogen bubbling for 30 min under magnetic stirring. The mixture was then heated in an oil bath at 353 K for 4 h under nitrogen atmosphere. At the end of the polymerization, water was evaporated under reduced pressure. Degree of polymerization (DP) and conversion were determined by ^{1}H NMR ($DP_{P(APEO)}$ = 25.4, monomer conversion > 99.2%). NMR sample preparation: 0.5 mL of D_2O was added to 0.1 mL of crude polymerization medium and quenched in liquid nitrogen. Determination of M_n, M_w and dispersity **Đ** was performed by size exclusion chromatography in THF (SEC-THF) with PMMA calibration (M_n = 8040 g.mol^{-1}, M_w = 9610 g.mol^{-1} and **Đ** = M_w/M = 1.19). The full characterization is given in Figures S2 and S3.

Synthesis of Poly(poly(ethylene glycol)-methyl ether acrylate)-*b*-poly(sodium 4-vinylbenzenesulfonate) by aqueous reversible addition-fragmentation chain transfer (RAFT) polymerization

The synthesis of the DHBC was adapted from previous works[28–30] and performed as follows: $P(APEO)_{25}$-DDMAT (15.02 g, 1.22 mmol, 1 eq), sodium 4-vinylbenzenesulfonate (SSNa, 6.92 g, 30.3 mmol, 24.3 eq), ACPA (0.0702 g, 0.25 mmol, 0.2 eq) and distilled water (9.15 g) were introduced in a round bottom flask and stirred (solids content= 70 %). The mixture was degassed with nitrogen bubbling for 30 min under magnetic stirring. The reaction medium was then heated in an oil bath at 353 K for 4 hours under nitrogen atmosphere. The resulting double hydrophilic block copolymer (DHBC) was then lyophilized. Degree of polymerization (DP) and conversion were determined by ^{1}H NMR ($DP_{P(SSNa)}$ = 21.4, monomer conversion > 99.9 %, $M_{n,\ P(APEO)\text{-}b\text{-}P(SSNa)}$ = 16 954 g.mol^{-1}, Figure S4). Due to the polyionic structure, no SEC analysis was realized on this DHBC but a capillary-electrophoresis (CE) experiment was performed (Figure S5), according to conditions previously reported,[30] to check the presence of the covalent link between the two blocks in synthesized $P(APEO)_{25}$-*b*-$P(SSNa)_{21}$-DDMAT.

Synthesis of the polyacid-functionalized silica material MesoPIC-PSS

MesoPIC-PSS particles were prepared following a one-pot synthesis approach. The concentrations of oligochitosan and TEOS were fixed with respect to the number of styrene sulfonate (SS) and ethylene oxide (EO) units of the PAPEO-*b*-P(SSNa) copolymer: molar ratios were set at 1 nitrogen per SS (N/SS = 1) and 1 silicon per EO (Si/EO = 1). The final concentration of the reaction medium was set at 2.0 wt% of DHBC polymer.

100 mg of PAPEO-*b*-P(SSNa) was dissolved in a mixture of 4.04 g of deionized water and 27.2 mg of oligochitosan. The pH of the solution was then adjusted to 2 using H_2SO_4 (1 M). Into the obtained clear solution, 244 mg of TEOS was added and the solution was stirred at 303 K for 1h. After that, the pH was rapidly increased to 4.5 with an aqueous NaOH solution (2 M). The mixture was stirred slowly for 5 hours at 303 K. The precipitate formed was then recovered by centrifugation, and dispersed in 12 ml of aqueous solution at pH=4.5 for 20 min to remove excess polymer. The product was centrifuged, the supernatant was eliminated, and the solid was dispersed and stirred for 16h in 12 ml of an aqueous solution with 0.05M H_2SO_4 and 1M NaCl. The dispersion was centrifuged and the process was repeated a first time for 3h with 12ml of an aqueous solution with 0.5M H_2SO_4 and 1M NaCl, and a second time for 1h with 12ml of an aqueous solution with 0.5M H_2SO_4 but without NaCl. Finally, the solid was recovered by centrifugation and air-dried at 353 K for 16 hours; typically, 100 mg of dry powder was obtained.

Characterization

Structural characterizations

TEM images were acquired on microtome cut samples using a JEOL 1200 EX II operating at 120 kV. Samples **SEM** images were obtained using a Hitachi S4800 FEG-HR operating at 5 kV. **SAXS** experiments were run using a homemade instrument with a copper X-ray tube (λ=1.54 Å). **Nitrogen sorption** analyses were performed at 77K using a Micromeritics Tristar 3000 after degassing samples one night at 353 K under secondary vacuum. The specific surface area was calculated using the BET equation in the range $0.15 < p/p° < 0.35$, volumes of micro- and mesopores were calculated using the alpha-S method, distributions of pore diameters were calculated on the adsorption branch of the sorption isotherm using Broekhoff and Boer equations.

Chemical characterization

TGA were performed using a PerkinElmer STA 6000 under air flow from 300 K to 1173 K with a 10 $K.min^{-1}$ rate. The silica content SiO_2 wt.% was determined as the residual final mass at 1173 K. **Elemental analyses** were performed on a Elementar Vario Micro Cube to determine C wt.%, S wt.% and N wt.%, respectively the mass content of carbon, sulfur and nitrogen. **TGA-MS** measurements were done with a Setaram STA-MS operating under air, from 303 K to 1173 K with a heating rate of 5 $K.min^{-1}$. **^{29}Si MAS NMR** experiments were run on a Varian VNMRS 400 MHz at 293K with a speed rotor rotation of 5 kHz. Pulses of $\pi/6$ were repeated every 60 s. Octa(dimethylsiloxy)-octasilsesquioxane (Q8M8) was used as the chemical shift reference (δ = -12,6 ppm). The **proton exchange capacity** was determined by titration of the H^+ in solution after ionic exchange with Na^+. Typically, 50 mg of MesoPIC material was added to 10 ml of an aqueous solution of sodium chloride (NaCl, 1M) and stirred for 24h at room temperature. The suspension was then filtered and the obtained solution was titrated with a sodium hydroxide aqueous solution (NaOH, 0.01M) using a pH-meter.

DLS analyses of PIC micelles were performed using a Malvern 4800 spectrogoniometer device with a laser source of 50 mW operating at 582 nm. Hydrodynamic diameters were obtained from autocorrelation functions fitted with CONTIN algorithm. Suspensions were prepared in deionized water with a concentration of PAPEO-*b*-P(SSNa) of 2wt.% and with a molar ratio between oligochitosan units and SSNa units of 1. The pH was adjusted at 4.5 with NaOH 2M solution. Analyses were performed without filtration.

Water adsorption. Water adsorption was performed at 298 K using a home-made apparatus.[31,32] In brief, this sorption device is based on manometric measurements of the

equilibrium water pressure before and after each sorption step. The pressure is recorded using two capacitive pressure gauges (10 and 1000 Torr). The whole device is placed in a climatic chamber allowing for a thermal stability better than 0.1 K at constant temperature (here, 298 K). The sample cell can be disconnected from the sorption line, allowing for an activation of the sample before the sorption measurements. The sorption thermodynamic equilibrium is ensured for each sorption step by setting a time criterion at 300s, which means that the pressure must remain constant for 300 s before recording the equilibrium pressure. Depending on the sorption process (monolayer sorption, capillary condensation, ...), equilibrium times are different and they can reach up to 600 min for a single step.[33]

Conductivity. The impedance measurements were carried out using a Solartron analytical Modulab XM MTS over a frequency range from 1Hz to 10^6 Hz with an *ac* applied voltage of 0.020 V. The powder sample was placed between two gold electrodes in a parallel plate capacitor configuration with an annular Teflon spacer to provide insulation, allowing the use of the "two-probe" method for the electrical measurements. The Relative Humidity (RH) and Temperature (T) were monitored by a 'Bench-Top type climatic chamber' from ESPEC Corporation. It is composed of a small liquid water "bath" located in the mixing plenum; as the chamber air is drawn into the plenum, it passes the bath, picking up vapor submitted to the sample. Impedance was recorded with varying RH from 35 to 95 %, while T was fixed in the [298 K – 363 K] range. The sample was equilibrated for at least 12 hours, before changing the RH/T conditions.

The resistance R of the solid was determined from the analysis of the Nyquist plots (-Z" = f(Z')), i.e. from the real-axis intercept of the signal and/or the fitting procedure with equivalent circuits using the ZView Software. In the latter case, the best fit was obtained considering the following equivalent circuit model:

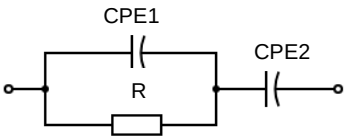

where R represents the bulk resistance, CPE1 and CPE2 refer to the constant phase elements for the non-ideal capacitance behaviors of the bulk solid and the electrodes, respectively. The conductivity values were obtained using $\sigma=1/R\times l/S$, where l and S are the sample thickness and surface, respectively. As shown in the impedance measurements section of SI, both approaches converge towards comparable values of σ, supporting that both methods can be equally considered. The conductivity values are given with an uncertainty of $\Delta\sigma/\sigma = 0.01$.

The activation energy associated with the proton transport process was deduced from the linear fitting of ln (σT) versus 1/T, according to the Arrhenius equation $\sigma(T) = \sigma_0/T \exp(-\Delta E/kT)$, where k is the Boltzmann constant.

Results and discussion

Scheme 1 describes the general concept of the functional material synthesis. First, a mesostructured PIC-silica hybrid phase is synthesized by macroscopic precipitation at room temperature in water at pH = 4.5 due to a cooperative organization between a $P(APEO)_{25}$-*b*-$P(SSNa)_{21}$ DHBC of well-defined block molecular weights synthesized by controlled radical polymerization (see Characterization of the DHBC section and Materials and Methods section in SI), a hydrosoluble renewable biomass oligochitosan and silicic species obtained by pre-hydrolysing TEOS used as a silica source. Formation of the hybrid phase results from electrostatic complexation between the SO_3^- functions of the DHBC and the NH_3^+ functions of oligochitosan, together with hydrogen bonding between the ethylene oxide units of the DHBC neutral blocks and the silanol groups of the silicic species. Upon dispersion of the hybrid material in an aqueous solution of hydrochloric acid (pH = 1) and sodium chloride (1 $mol.L^{-1}$), the electrostatic interactions between the polyions are disrupted, which ensures the dissociation of PIC micelles. The objective is threefold: (i) elute the oligochitosan for potential reuse (recycling of the micellization auxiliary),[25] (ii) generate mesoporosity in the material, (iii) decorate the mesopore walls with accessible sulfonic acid-rich polyions. The PAPEO chains of the copolymer remain anchored to the silica walls via hydrogen bonds, allowing dense and homogeneous functionalization of the mesopores with the PSS polyacid chains.

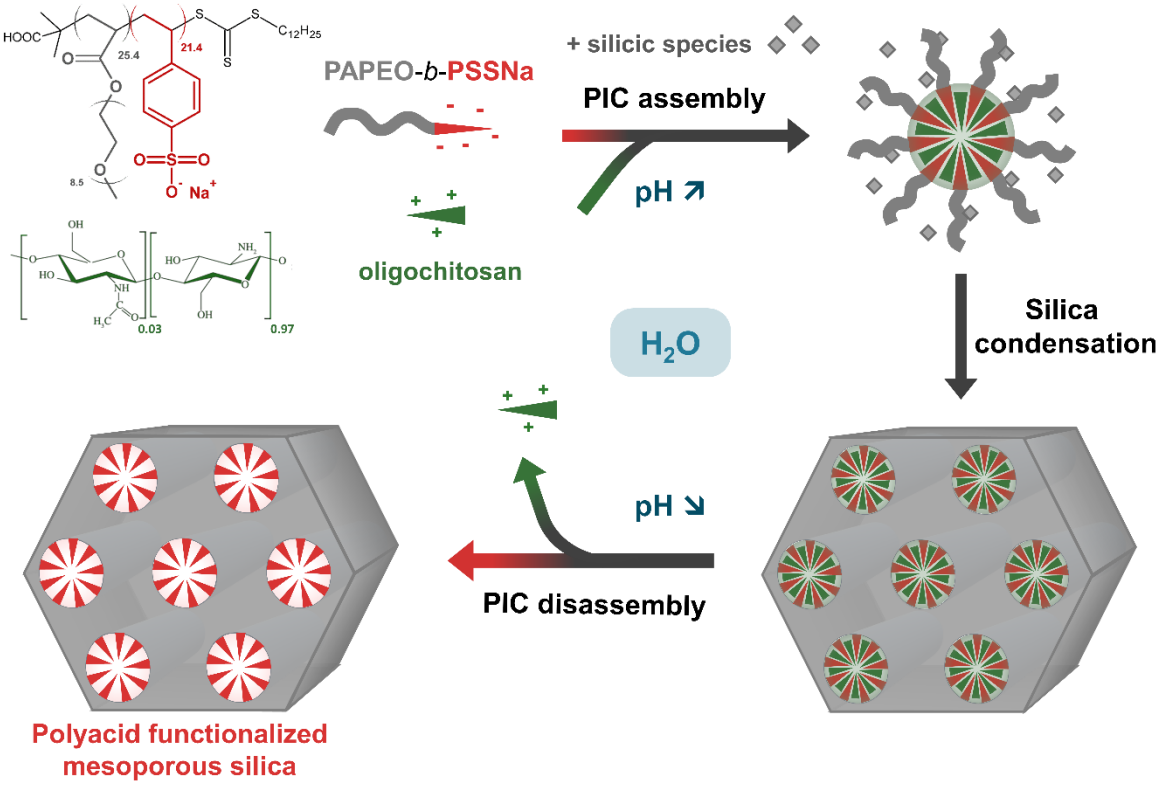

Scheme 1: Illustration of the eco-designed pathway to form large-pore ordered silica functionalized with polyacid chains, called MesoPIC-PSS

The PSS-functionalized silica material (MesoPIC-PSS) exhibits a long-range ordered 2D hexagonal structure. TEM images of the particles sectioned by ultra-microtome cutting reveal the ordered hexagonal network of the cylindrical mesopores (Figure 1a, supplementary images on Figure S6). The SAXS pattern shows four well-defined peaks, indicating the long-range order of the P6mm mesostructure with a d0 spacing of 14.9 nm (Figure 1b). SEM images reveal the long-range ordered internal structure in micrometer-sized particles (Figures 1c and S7).

The chemical composition of MesoPIC-PSS was determined by combining thermogravimetric analysis (TGA) and elemental analysis (EA). According to TGA, the residual mass recorded at T = 1173 K corresponds to 47 wt.% of silica. ^{29}Si MAS NMR analysis (Figure 1d) reveals that 51 %, 46 % and 3 % of Q_4, Q_3 and Q_2 species respectively, constitute the silica framework, resulting in an overall formula of $SiO_{1.74}(OH)_{0.52}$. It should be noted that a silanol-rich MesoPIC-PSS was successfully synthesized in this way in conjunction with the absence of any calcination step during the elaboration process. Most importantly, the nitrogen content measured from the EA (< 0.1 wt. %N, Table S1) highlights a complete removal of oligochitosan from the elution process, ensuring the complete decomplexation of sulfonic acid functions.

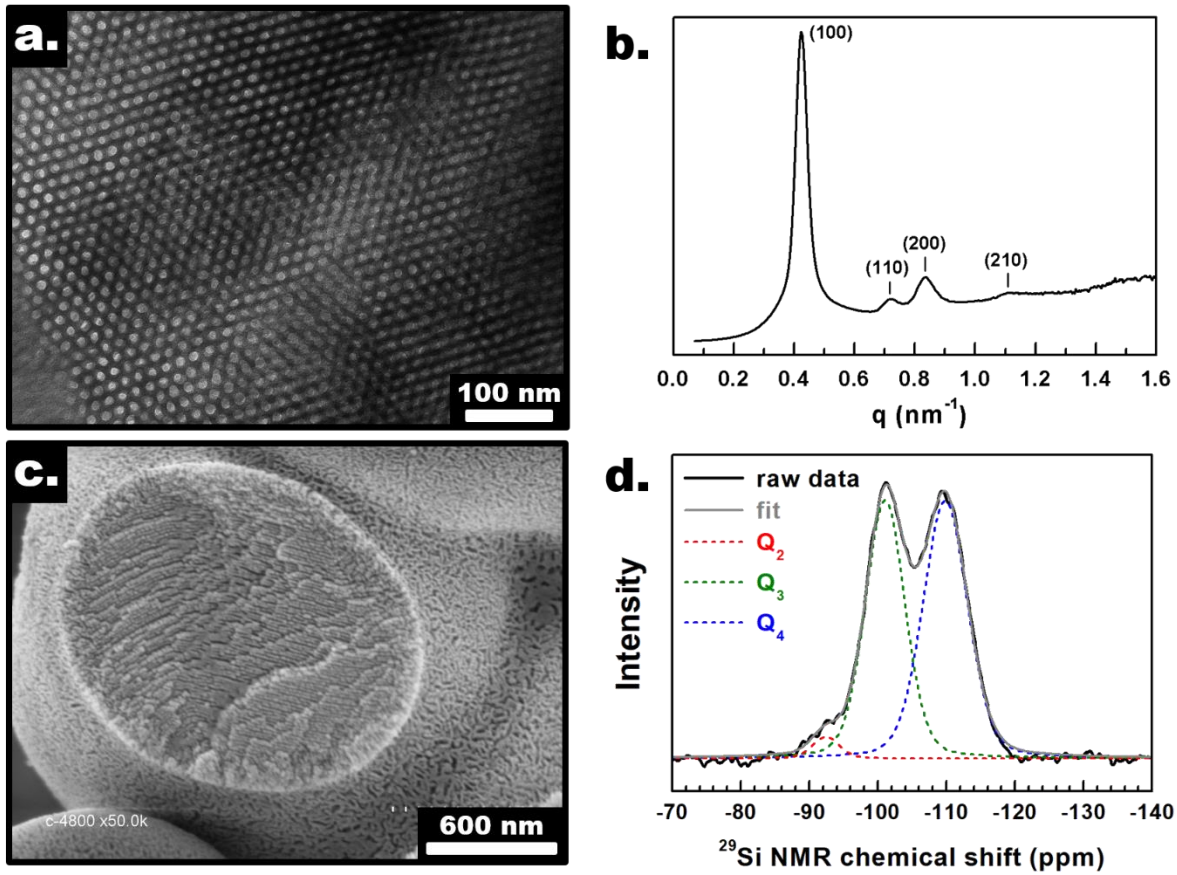

Figure 1: a) TEM image, b) SAXS pattern, c) SEM image, and d) ^{29}Si one-pulse MAS NMR spectrum of MesoPIC-PSS. Q_2, Q_3 and Q_4 refer to $Si(OH)_2(OSi)_2$, $Si(OH)(OSi)_3$ and $Si(OSi)_4$ species respectively.

According to EA, the MesoPIC-PSS material contains a large amount of PAPEO-*b*-PSS in the mesopores (886 $mg.g^{-1}_{SiO2}$, Table 1), which corresponds to 99% of the DHBC polymers initially present in the hybrid MesoPIC material. This key feature ensures an intrinsically dense and homogeneous spatial distribution of the polyacid chains in the mesopores considering that: (i) the PAPEO-*b*-PSS polymers associated with oligochitosan are the pore structuring agents, and (ii) they remain in the silica-based material during the PIC disassembly process. The density of sulfonic acid functions was calculated to be 1.16 $mmol.g^{-1}_{SiO2}$ or 0.54 $mmol.g^{-1}_{material}$, which is within the range of those reported in the literature for mesoporous silica particles functionalized with *mono*- or *poly*sulfonic acid. Table S2 lists the relevant sulfonic acid-functionalized OMS in particle or thin film form, including their density of sulfonic acid functions as well as their textural properties. Among them, sulfonic acid-functionalized mesoporous silica thin films synthesized by Fujita et al. exhibit the highest density of sulfonic acid functions.[19] The chemical composition of the copolymer in the material was preserved, as indicated by the similar value of the C/S mass ratio in the final material (9.8) compared to that of the raw PAPEO-*b*-PSS copolymer (10.5). Most importantly, the volume density of SO_3H

functions in the mesopores reaches 1 function per nm^3 of mesopore volume, which is the highest value reported to date for mesoporous particles (calculations are provided in ESI together with comparisons to values for other materials in the literature, Table S2). In addition, the acidic protons in MesoPIC-PSS are highly accessible: 80% of them were exchanged in aqueous solution, giving an exchange capacity of 0.44 $mmol_{H^+}.g^{-1}_{material}$. This result contrasts with a previous report of a PSS-functionalized SBA-15, in which only 14% of the acidic functions were accessible to ion exchange due to the hydrophobicity of the material.[5] In our case, the excellent accessibility may be the consequence of (i) the high hydrophilicity of MesoPIC-PSS due to the numerous silanol and SO_3H functions, and (ii) the homogeneous distribution of the polymer chains within the pores. Therefore, the present strategy provides mesoporous materials with large pores, high pore volume and very high volume density of accessible and strong acid functions in the mesopores.

Table 1: Textural properties and chemical composition of MesoPIC-PSS.

V_{micro} / $cm^3.g^{-1}$	V_{meso} / $cm^3.g^{-1}$ [a]	d_{meso} / nm [b]	d_0 / nm [c]	t_{wall} / nm [d]	S_{BET} / $m^2.g^{-1}$	$mg_{DBHC}.g_{SiO2}^{-1}$ [e]	$mmol_{-SO3H}.g_{SiO2}^{-1}$ [e]
0.00	0.24	10.0	14.9	7.2	105	886	1.16

[a] Total pore volume at p/p° = 0.975 [b] mean mesopore diameter at adsorption [c] lattice parameter [d] thickness of silica walls [e] Determined by elemental analysis and TGA.

The dynamic thermal stability of MesoPIC-PSS was evaluated under air by TGA coupled with mass spectrometry (TGA-MS, Figure S8). The PAPEO-*b*-PSS copolymer decomposes from 475 K to 950 K in the material, generating CO_2, H_2O and SO_2. The thermal decomposition of PAPEO-*b*-PSS occurs in the same temperature range (Figure S9), indicating that the thermal stability of the copolymer is not affected by the mesoporous structure, probably due to the highly porous structure and large diameter of the mesopores.

The accessibility to these large pores from the outer surface of the particles is clearly evident in the SEM images in Figure 1c. The sharp symmetric hysteresis loop of the type IV nitrogen sorption isotherm (Figure 2a) further validates the accessibility and homogeneity of the mesoporosity in the particles. Capillary condensation of nitrogen occurs in MesoPIC-PSS in the same manner as in the case of polymer-free OMS (calcined material), suggesting that nitrogen sorption is not affected by the presence of polymers in the mesopores (Table 1). The pore size distribution indicates monodisperse mesopores of 10.0 nm in diameter. A consistent diameter (10.5 nm) was estimated by analyzing the TEM images (Figure S10), from which the pores are distinctly delineated from the silica walls, confirming the fact that nitrogen sorption analysis

allows access to the mesopore diameter as if no polymers were present. Given the presence of many functional polymers in the mesopores and the large thickness of the silica walls (7 nm, Table 1), the mesopore volume (V_{meso}) of 0.24 cm^3. $g^{-1}_{material}$ can be described as really high. No microporosity could be detected by *t*-plot in contrast to SBA-15-type materials, in which micropores are generated by removal of the micelle PEO corona by calcination.[34] In the present approach, the stable anchoring of the comb-type PAPEO blocks in the silica walls and the absence of any calcination step avoid microporosity formation.

In summary, the MesoPIC process can produce porous silica-based solids with both high porosity and a high degree of functionalization. On one hand, the pore volume, which results from the elution of the oligochitosan, is related to the amount of oligochitosan initially incorporated into the material. On the other hand, the degree of functionalization of the MesoPIC-PSS material is related to the amount of block copolymer incorporated in the material. Knowing that the core of the PIC assembly results from the charge compensation between the PSS and the oligochitosan, this suggests that the pore volume and the degree of PSS functionalization should both concomitantly increase when the length of the PSS block is increased. This represents a major advantage over the former grafting post-functionalization approaches, in which an increase in polymer block length or degree of grafting inherently leads to a decrease in pore volume.

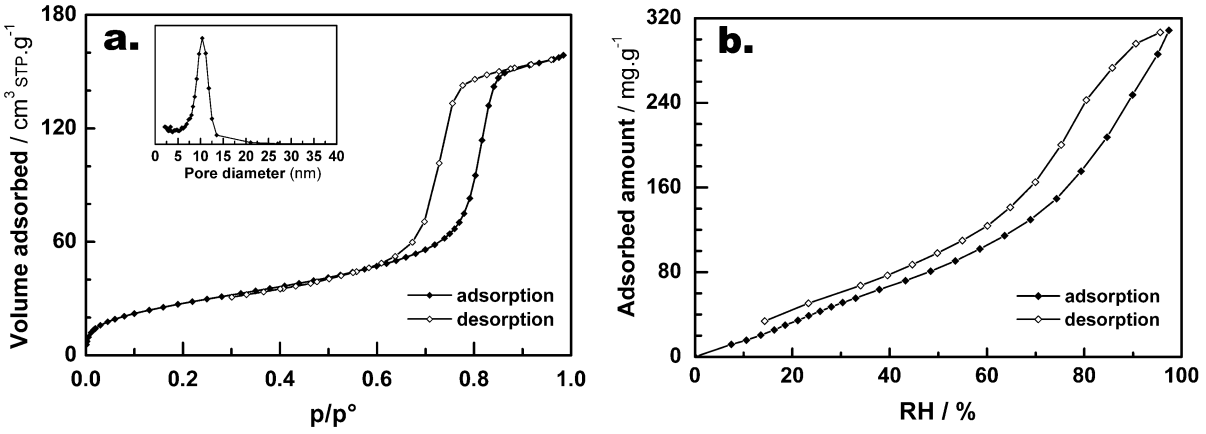

Figure 2: MesoPIC-PSS sorption isotherms of a) nitrogen measured at 77K and related pore size distribution, and b) water measured at 298 K.

Water sorption analyses were performed to evaluate the water sorption capacity and affinity of the functional surfaces for water, which can then be related to proton conductivity properties. The water vapor sorption isotherm recorded at 298 K is shown in Figure 2b. The maximum water uptake at RH = 97% reaches 308 $mg_{H2O}.g^{-1}_{material}$. The linear shape at low

relative pressure is characteristic of a mixture of type IV and V sorption isotherms,[35] as previously reported for bare and sulfonic functionalized mesoporous silica.[36,37] Maaz *et al*. proposed using the water pore filling volume ratio at $p/p°$ = 0.1 as an indicator of the hydrophilicity of the material, which has been shown to increase with silanol density and microporosity.[36] For MesoPIC-PSS, the water pore filling volume ratio at $p/p°$ = 0.1 was calculated to be 0.06, which is one of the highest values of all materials reported by Maaz *et al*.[36] Since no microporosity was found for MesoPIC-PSS, the strong hydrophilicity is due either to the presence of the many silanols revealed by ^{29}Si MAS NMR (see above), the large number of sulfonic acid functions or most likely a combination of both. A comparison of the water and nitrogen sorption isotherms provides useful insights. A clear difference in the isotherms appears at intermediate RH levels. The high uptake in this region can been attributed to a capillary condensation process in the case of nitrogen adsorption; however, in the case of water adsorption, the curve is not as steep in the region of intermediate RH levels. In addition, water uptake increases gradually up to saturation. This could be related to the adsorption of water molecules onto the many sulfonic acid groups of the polymeric chains, as usually observed for Proton Exchange Membranes (PEM).[38] For example, perfluorosulfonic acid membranes with hydrophobic and hydrophilic domains show no capillary condensation of water, which first condenses on the sulfonic acid groups before percolation.[38–40] In contrast, nitrogen, which has no specific affinity for the polymer, condenses as it does in the pores of bare mesoporous silica. This would explain the larger volume of water adsorbed (0.31 $cm^3.g^{-1}$) compared to nitrogen (0.24 $cm^3.g^{-1}$). Since MesoPIC-PSS has both a hydrophilic silica surface and hydrophilic PSS blocks, one would expect water molecules to adsorb onto both types of sites and condense *via* a combination of the mechanisms reported for bare mesoporous silica and PEM. The structuration of the polymer chains in the mesopores could also play a role in the differences between nitrogen and water adsorption isotherms. While at 77K these chains are rigid and cover the surface of the mesopore walls, at 298 K, the polymer chains are flexible and can adopt a brush-like conformation. In the first case, the mesoporosity is fully accessible to nitrogen and capillary condensation can therefore occur according to the Kelvin's law. In the second case, the presence of polymer chains in the mesopores prevents the formation of a homogeneous meniscus of water in the mesopores, which is a prerequisite for homogeneous capillary condensation. Therefore, the mesopores can be progressively filled with water as the relative pressure increases. Because of the inflection of the water adsorption isotherm noticeable at 60% RH, capillary condensation probably occurs between 60% RH and 95% RH. Still, further experiments or simulations are needed to confirm these interpretations.

Given the thermal stability of the inorganic framework, the well-defined mesoporous structure, the dense functionalization and the numerous silanol functions, MesoPIC-PSS

appears to be a promising candidate for proton conductivity applications.[41,42] *AC* impedance spectroscopy was used to explore its proton conductivity at 95% Relative Humidity for temperatures ranging from 298 K to 363 K. The Nyquist plots are shown in Figure 3a. They correspond to very low impedances and are dominated by the capacitive tail due to the ionic-blocking electrodes. The total impedance was extrapolated from the linear region to the real axis. The corresponding conductivity values increase from 2.5 x 10^{-3} S.cm^{-1} to 2.4 x 10^{-2} S.cm^{-1} upon heating from 298 K to 363 K, illustrating the superprotonic conductivity behavior of MesoPIC-PSS ($\sigma > 10^{-4}$ S.cm^{-1}).[43] Interestingly, the performances of MesoPIC-PSS exceed that of the best sulfonic acid based OMS particles ($\boldsymbol{\sigma^{H^+}_{363K,100\%RH} = 1.10^{-2}\ S.cm^{-1}}$), while exhibiting a larger pore diameter (Table S3). Furthermore, the outstanding performance recorded at 363 K and 95% RH is maintained over at least one week (Figure 3b), highlighting the long-term hydrothermal stability of the silica at the T/RH operating conductivity conditions. This is further highlighted by the comparable TEM images of the material collected before and after the impedance measurements (Figure S11). These results confirm the robustness and high hydrothermal stability of MesoPIC-PSS, which can be attributed to the thick walls of the material and the absence of any microporosity.

The activation energy for proton transfer in MesoPIC-PSS was deduced from an Arrhenius plot (Figure 3c). It reaches 0.28 eV, which is consistent with a Grotthuss transfer mechanism ($\Delta E <$ 0.40 eV).[44] It is assumed that protons are transferred from -SO_3H groups to water molecules interacting through hydrogen-bonds, creating a pathway for proton migration into the silica porosity. To verify that water assists the proton transfer, the humidity dependence of the conductivity for MesoPIC-PSS was studied at 298 K and 363 K (see Figures S12-S14 and Table S4). The significant increase in conductivity with increasing humidity, from 40 % to 95 % of RH, confirms that H_2O molecules are involved in the proton migration mechanism, and this trend is valid regardless of the temperature. Propitiously, the dependence of conductivity with relative humidity perfectly follows the water uptake profile obtained from the manometric adsorption isotherm (Figure 3d). This excellent correlation confirms that the water-mediated proton conductivity of MesoPIC-PSS is proportional to the concentration of adsorbed water molecules inside the porosity, which are assumed to act as charge carriers through the path they create via the H-bond network.[45] Noteworthy, conductivity measurements recorded at 303 K as a function of RH perfectly illustrates the acid character of the protogenic groups of the MesoPIC-PSS. This also provides evidence that the proton conduction process occurs through the intrinsic bulk solid, *i.e.* through the water-filled pores of the silica particles, and not through the grain boundaries or interparticle domains.[46–49]

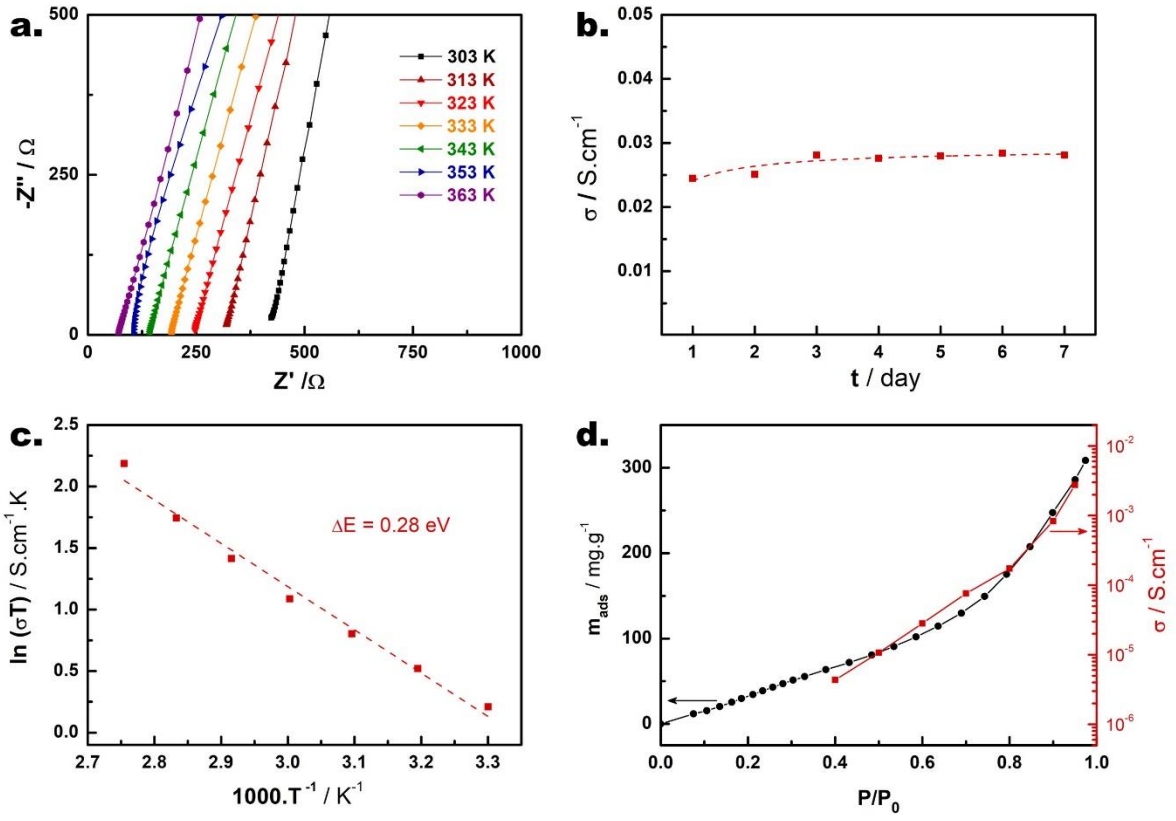

Figure 3: a) Nyquist plots of the impedance for MesoPIC-PSS recorded under 95% RH for temperature varying from 298 K to 363 K. b) Long term stability of the conductivity of MesoPIC-PSS at 363 K/95% RH. The dashed curve is a guide for the eye. c) Arrhenius type plot of the conductivity for MesoPIC-PSS under 95 % RH. The dashed line corresponds to the linear least-square fit. d) Evolution of the water mass uptake (black circle) and the conductivity (red squares) for MesoPIC-PSS versus the water relative pressure at 298 K upon adsorption.

Conclusions

An environmentally friendly integrated strategy has been developed to prepare ordered mesoporous silica functionalized with strong polyacid chains that are densely and homogeneously distributed in the mesopores, allowing the preparation of superprotonic conductors. The synthesis process takes place in an aqueous solvent at room temperature and relies on the use of complex micelles of oppositely charged hydrophilic polymers. A functional polyacid DHBC complexed with an oligoamine (oligochitosan) was used to direct the structure of silica into an ordered 2D hexagonal mesostructure with large mesopores of 10 nm diameter. The oligoamine was then released into water by changing the pH and ionic strength, generating mesoporosity and revealing the acidic functions. More than 99% of poly(styrene sulfonic acid) chains remained anchored in the material during the PIC dissociation step,

demonstrating the high efficiency of the process resulting in an inherently dense and homogeneous distribution of functional polymers along the mesopores. The PSS chains have a known and well-defined degree of polymerization of 21, which leads to a large amount of acid functions in mesopores: 1.16 mmol per gram of silica, which corresponds to the highest volume density reported so far of 1 SO_3H function per nm^3 of mesopore volume. The success of this direct and integrated strategy can be attributed to (i) the use of PIC micelles as structuring, pore-forming and functionalizing agents, and (ii) the selectivity of the elution process that allows the removal of the oligoamine while keeping the totality of the functional copolymers in the mesopores. Moreover, overcoming performance-limiting inhomogeneities, we designed a superprotonic conductor: the sulfonic acid functionalized MesoPIC-PSS material exhibits superprotonic conductivity, up to 0.024 S cm^{-1} at 95% RH and 363 K, with a Grotthus-like mechanism. This performance was extremely stable for at least seven days, due to the high hydrothermal stability of the mesoporous hybrid material characterized by thick silica walls, large pores and no microporosity.

These results demonstrate for the first time the major interest of stable large pore mesoporous materials functionalized by dense and homogeneous brushes of strong polyacids as solid-state proton electrolytes. Moreover, this strategy could be adapted to design Li- or Na-ion conducting materials. Furthermore, the versatility of the process can be easily exploited to control the ordered silica structure and to tune the pore properties of functionalized hybrid materials through the reactivity of PIC micelles to pH, concentration or ionic strength.[23,24] Overall, our synthesis strategy paves the way for the large-scale sustainable development of well-defined polymer-functionalized mesoporous materials.

Acknowledgments

The authors thank Thomas Cacciaguerra for TEM analysis at the University of Montpellier and Didier Cot for SEM analysis at the European Institute of Membranes; they also acknowledge Philippe Gaveau and Emmanuel Fernandez for NMR experiments, Philippe Dieudonné for SAXS analysis and Amine Geneste for TG-MS analysis (University of Montpellier). The electrical measurements were performed with the support of the Balard Plateforme d'Analyses et de Caractérisation (PAC Balard). This work was supported by the ANR MESOPIC project (ANR-15-CE07-0005) and the ANR PASSCATA project (ANR-16-CE07-0029-02).

Supporting Information description

Supporting information includes: characterization of the DHBC by ^{1}H NMR, SEC-THF and capillary-electrophoresis, supplementary images of MesoPIC-PSS particles, chemical composition of MesoPIC-PSS, comparison of the density of acid functions in MesoPIC-PSS with those of representative functional porous silica particles, calculations of the density of functions in mesopores, evaluation of dynamic thermal stability of MesoPIC-PSS by TG-MS, determination of pore size on TEM image, comparison of MesoPIC-PSS protonic conductivity with those of representative functional porous silica, evaluation of the stability of MesoPIC-PSS at high temperature and relative humidity, impedance measurements.

References

(1) Soler-Illia, G. J. A. A.; Azzaroni, O. Multifunctional Hybrids by Combining Ordered Mesoporous Materials and Macromolecular Building Blocks. *Chem. Soc. Rev.* **2011**, *40* (2), 1107. https://doi.org/10.1039/c0cs00208a.

(2) Brilmayer, R.; Förster, C.; Zhao, L.; Andrieu-Brunsen, A. Recent Trends in Nanopore Polymer Functionalization. *Curr. Opin. Biotechnol.* **2020**, *63*, 200–209. https://doi.org/10.1016/j.copbio.2020.03.005.

(3) Ngo, T. T. T.; Besson, E.; Bloch, E.; Bourrelly, S.; Llewellyn, R.; Gastaldi, S.; Llewellyn, P. L.; Gigmes, D.; Phan, T. N. T. One-Pot Synthesis of Organic Polymer Functionalized Mesoporous Silicas. *Microporous Mesoporous Mater.* **2021**, *319*. https://doi.org/10.1016/j.micromeso.2021.111036.

(4) Li, C.; Yang, J.; Wang, P.; Liu, J.; Yang, Q. An Efficient Solid Acid Catalyst: Poly-p-Styrenesulfonic Acid Supported on SBA-15 via Surface-Initiated ATRP. *Microporous Mesoporous Mater.* **2009**, *123* (1–3), 228–233. https://doi.org/10.1016/j.micromeso.2009.04.005.

(5) Martín, A.; Morales, G.; Martínez, F.; van Grieken, R.; Cao, L.; Kruk, M. Acid Hybrid Catalysts from Poly(Styrenesulfonic Acid) Grafted onto Ultra-Large-Pore SBA-15 Silica Using Atom Transfer Radical Polymerization. *J. Mater. Chem.* **2010**, *20* (37), 8026. https://doi.org/10.1039/c0jm01589j.

(6) Jiang, T.; Huang, Q.; Li, Y.; Fang, M.; Zhao, Q. Catalytic Performance of Strong Acid Catalyst: Methyl Modified SBA-15 Loaded Perfluorinated Sulfonic Acid Obtained by the Waste Perfluorinated Sulfonic Acid Ion Exchange Membrane. *J. Solid State Chem.* **2018**, *258* (August 2017), 602–609. https://doi.org/10.1016/j.jssc.2017.11.027.

(7) Ma, Z.-H.; Han, H.-B.; Zhou, Z.-B.; Nie, J. SBA-15-Supported Poly(4-Styrenesulfonyl(Perfluorobutylsulfonyl)Imide) as Heterogeneous Brønsted Acid

Catalyst for Synthesis of Diindolylmethane Derivatives. *J. Mol. Catal. A Chem.* **2009**, *311* (1–2), 46–53. https://doi.org/10.1016/j.molcata.2009.06.021.

(8) Alghamdi, A. A.; Mrair, Y. M.; Alharthi, F. A.; Al-Odayni, A. B. Catalytic Performance of SBA-15-Supported Poly (Styrenesulfonic Acid) in the Esterification of Acetic Acid with n-Heptanol. *Appl. Sci.* **2020**, *10* (17). https://doi.org/10.3390/app10175835.

(9) Calvo, A.; Yameen, B.; Williams, F. J.; Azzaroni, O.; Soler-Illia, G. J. A. A. Facile Molecular Design of Hybrid Functional Assemblies with Controllable Transport Properties: Mesoporous Films Meet Polyelectrolyte Brushes. *Chem. Commun.* **2009**, No. 18, 2553. https://doi.org/10.1039/b822489g.

(10) Tom, J. C.; Appel, C.; Andrieu-Brunsen, A. Fabrication and in Situ Functionalisation of Mesoporous Silica Films by the Physical Entrapment of Functional and Responsive Block Copolymer Structuring Agents. *Soft Matter* **2019**, *15* (40), 8077–8083. https://doi.org/10.1039/C9SM00872A.

(11) Yuan, L.; Tang, Q.; Yang, D.; Zhang, J. Z.; Zhang, F.; Hu, J. Preparation of PH-Responsive Mesoporous Silica Nanoparticles and Their Application in Controlled Drug Delivery. *J. Phys. Chem. C* **2011**, *115* (20), 9926–9932. https://doi.org/10.1021/jp201053d.

(12) Samart, C.; Prawingwong, P.; Amnuaypanich, S.; Zhang, H.; Kajiyoshi, K.; Reubroycharoen, P. Preparation of Poly Acrylic Acid Grafted-Mesoporous Silica as PH Responsive Releasing Material. *J. Ind. Eng. Chem.* **2014**, *20* (4), 2153–2158. https://doi.org/10.1016/j.jiec.2013.09.045.

(13) Yang, G.; Xu, L.; Xu, J.; Zhang, R.; Song, G.; Chao, Y.; Feng, L.; Han, F.; Dong, Z.; Li, B.; Liu, Z. Smart Nanoreactors for PH-Responsive Tumor Homing, Mitochondria-Targeting, and Enhanced Photodynamic-Immunotherapy of Cancer. *Nano Lett.* **2018**, *18* (4), 2475–2484. https://doi.org/10.1021/acs.nanolett.8b00040.

(14) Li, Z.; Yao, Y.; Wang, D.; Hasan, M. M.; Suwansoontorn, A.; Li, H.; Du, G.; Liu, Z.; Nagao, Y. Simple and Universal Synthesis of Sulfonated Porous Organic Polymers with High Proton Conductivity. *Mater. Chem. Front.* **2020**, *4* (8), 2339–2345. https://doi.org/10.1039/d0qm00276c.

(15) Mikhailenko, S.; Desplantier-Giscard, D.; Danumah, C.; Kaliaguine, S. Solid Electrolyte Properties of Sulfonic Acid Functionalized Mesostructured Porous Silica. *Microporous Mesoporous Mater.* **2002**, *52* (1), 29–37. https://doi.org/10.1016/S1387-1811(02)00275-5.

(16) Marschall, R.; Rathouský, J.; Wark, M. Ordered Functionalized Silica Materials with High Proton Conductivity. *Chem. Mater.* **2007**, *19* (26), 6401–6407. https://doi.org/10.1021/cm071164i.

(17) Marschall, R.; Bannat, I.; Feldhoff, A.; Wang, L.; Lu, G. Q.; Wark, M. Nanoparticles of Mesoporous SO3H-Functionalized Si-MCM-41 with Superior Proton Conductivity. *Small* **2009**, *5* (7), 854–859. https://doi.org/10.1002/smll.200801235.

(18) Bibent, N.; Mehdi, A.; Silly, G.; Henn, F.; Devautour-Vinot, S. Proton Conductivity versus Acidic Strength of One-Pot Synthesized Acid-Functionalized SBA-15 Mesoporous Silica.

Eur. J. Inorg. Chem. **2011**, *2011* (21), 3214–3225. https://doi.org/10.1002/ejic.201100186.

(19) Fujita, S.; Koiwai, A.; Kawasumi, M.; Inagaki, S. Enhancement of Proton Transport by High Densification of Sulfonic Acid Groups in Highly Ordered Mesoporous Silica. *Chem. Mater.* **2013**, *25* (9), 1584–1591. https://doi.org/10.1021/cm303950u.

(20) Kruk, M. Surface-Initiated Controlled Radical Polymerization in Ordered Mesoporous Silicas. *Isr. J. Chem.* **2012**, *52* (3–4), 246–255. https://doi.org/10.1002/ijch.201100121.

(21) Yang, Q. H.; Ma, Z. H.; Ma, J. Z.; Nie, J. Mesoporous Silica Supported Water-Stable Perfluorobutylsulfonylimide and Its Catalytic Applications in Esterification. *Microporous Mesoporous Mater.* **2013**, *172*, 51–60. https://doi.org/10.1016/j.micromeso.2013.01.008.

(22) Paris, E.; Oldani, C.; Aricò, A. S.; D'Urso, C.; Bigi, F.; Maestri, G.; Pancrazzi, F.; Maggi, R. Silica Nanoparticles Decorated with Polymeric Sulfonic Acids Trigger Selective Oxidation of Benzylic Methylenes to Aldehydic and Ketonic Carbonyls. *ACS Sustain. Chem. Eng.* **2019**, *7* (6), 5886–5891. https://doi.org/10.1021/acssuschemeng.8b05845.

(23) Houssein, D.; Warnant, J.; Molina, E.; Cacciaguerra, T.; Gérardin, C.; Marcotte, N. Mesoporous Silica Templated by Polyion Complex Micelles: A Versatile Approach for Controlling the Mesostructure. *Microporous Mesoporous Mater.* **2017**, *239*, 244–252. https://doi.org/http://dx.doi.org/10.1016/j.micromeso.2016.10.013.

(24) Molina, E.; Mathonnat, M.; Richard, J.; Lacroix-Desmazes, P.; In, M.; Dieudonné, P.; Cacciaguerra, T.; Gérardin, C.; Marcotte, N. PH-Mediated Control over the Mesostructure of Ordered Mesoporous Materials Templated by Polyion Complex Micelles. *Beilstein J. Nanotechnol.* **2019**, *10* (1), 144–156. https://doi.org/10.3762/bjnano.10.14.

(25) Baccile, N.; Reboul, J.; Blanc, B.; Coq, B.; Lacroix-Desmazes, P.; In, M.; Gerardin, C. Ecodesign of Ordered Mesoporous Materials Obtained with Switchable Micellar Assemblies. *Angew. Chemie* **2008**, *47* (44), 8433–8437. https://doi.org/10.1002/anie.200802431.

(26) Richard, J.; Phimphachanh, A.; Jamet-Fournier, A.; Cacciaguerra, T.; Dieudonné-George, P.; Cot, D.; Destarac, M.; Lacroix-Desmazes, P.; In, M.; Marcotte, N.; Gérardin, C. Dual Control of External Surface and Internal Pore Structure of Small Ordered Mesoporous Silica Particles Directed by Mixed Polyion Complex Micelles. *Microporous Mesoporous Mater.* **2022**, *338*. https://doi.org/10.1016/j.micromeso.2022.111915.

(27) Ma, Z.; Lacroix-Desmazes, P. Synthesis of Hydrophilic/CO2-Philic Poly(Ethylene Oxide)-b-Poly(1,1,2,2-Tetrahydroperfluorodecyl Acrylate) Block Copolymers via Controlled/Living Radical Polymerizations and Their Properties in Liquid and Supercritical CO2. *J. Polym. Sci. Part A Polym. Chem.* **2004**, *42* (10), 2405–2415. https://doi.org/10.1002/pola.20117.

(28) Bathfield, M.; Warnant, J.; Gérardin, C.; Lacroix-Desmazes, P. Asymmetric Neutral, Cationic and Anionic PEO-Based Double-Hydrophilic Block Copolymers (DHBCs):

Synthesis and Reversible Micellization Triggered by Temperature or PH. *Polym. Chem.* **2015**, *6* (8), 1339–1349. https://doi.org/10.1039/c4py01502a.

(29) Molina, E.; Warnant, J.; Mathonnat, M.; Bathfield, M.; In, M.; Laurencin, D.; Jérôme, C.; Lacroix-Desmazes, P.; Marcotte, N.; Gérardin, C. Drug–Polymer Electrostatic Complexes as New Structuring Agents for the Formation of Drug-Loaded Ordered Mesoporous Silica. *Langmuir* **2015**, *31* (47), 12839–12844. https://doi.org/10.1021/acs.langmuir.5b03221.

(30) Phimphachanh, A.; Chamieh, J.; Leclercq, L.; Harrisson, S.; Destarac, M.; Lacroix-Desmazes, P.; Gérardin, C.; In, M.; Cottet, H. Characterization of Diblock Copolymers by Capillary Electrophoresis: From Electrophoretic Mobility Distribution to Distribution of Composition. *Macromolecules* **2020**, *53* (1), 334–345. https://doi.org/10.1021/acs.macromol.9b01978.

(31) Trens, P.; Belarbi, H.; Shepherd, C.; Gonzalez, P.; Ramsahye, N. A.; Lee, U. H.; Seo, Y. K.; Chang, J. S. Adsorption and Separation of Xylene Isomers Vapors onto the Chromium Terephthalate-Based Porous Material MIL-101(Cr): An Experimental and Computational Study. *Microporous Mesoporous Mater.* **2014**, *183*, 17–22. https://doi.org/10.1016/j.micromeso.2013.08.040.

(32) Fertier, L.; Théron, C.; Carcel, C.; Trens, P.; Wong Chi Man, M. PH-Responsive Bridged Silsesquioxane. *Chem. Mater.* **2011**, *23* (8), 2100–2106. https://doi.org/10.1021/cm103327y.

(33) Trung, T. K.; Déroche, I.; Rivera, A.; Yang, Q.; Yot, P.; Ramsahye, N.; Vinot, S. D.; Devic, T.; Horcajada, P.; Serre, C.; Maurin, G.; Trens, P. Hydrocarbon Adsorption in the Isostructural Metal Organic Frameworks MIL-53(Cr) and MIL-47(V). *Microporous Mesoporous Mater.* **2011**, *140* (1–3), 114–119. https://doi.org/10.1016/j.micromeso.2010.09.003.

(34) Kruk, M.; Jaroniec, M.; Ko, C. H.; Ryoo, R. Characterization of the Porous Structure of SBA-15 . *Chem. Mater.* **2000**, *12* (7), 1961–1968. https://doi.org/10.1021/cm000164e.

(35) K. S. W. Sing, D. H. Everett, R. A. W. Haul, L. Moscou, R. A. Pieroti, J. Rouquerol, T. S. Reporting Physisorption Data for Gas/Solid Systems with Special Reference to the Determination of Surface Area and Porosity (Recommendations 1984). *Pure Appl. Chem.* **1985**, *57* (4), 603–619. https://doi.org/10.1351/pac198557040603.

(36) Maaz, S.; Rose, M.; Palkovits, R. Systematic Investigation of the Pore Structure and Surface Properties of SBA-15 by Water Vapor Physisorption. *Microporous Mesoporous Mater.* **2016**, *220*, 183–187. https://doi.org/https://doi.org/10.1016/j.micromeso.2015.09.005.

(37) Timm, J.; Marschall, R. A Novel and Versatile Grafting Procedure: Toward the Highest Possible Sulfonation Degree of Mesoporous Silica. *Adv. Sustain. Syst.* **2018**, *2* (3), 1700170. https://doi.org/10.1002/adsu.201700170.

(38) Legras, M.; Hirata, Y.; Nguyen, Q. T.; Langevin, D.; Métayer, M. Sorption and Diffusion Behaviors of Water in Nafion 117 Membranes with Different Counter Ions. *Desalination*

2002, *147* (1–3), 351–357. https://doi.org/10.1016/S0011-9164(02)00608-2.

(39) Tsonos, C.; Apekis, L.; Pissis, P. Water Sorption and Dielectric Relaxation Spectroscopy Studies in Hydrated Nafion (-SO3K) Membranes. *J. Mater. Sci.* **2000**, *35* (23), 5957–5965. https://doi.org/10.1023/A:1026782509106.

(40) Wu, X.; Wang, X.; He, G.; Benziger, J. Differences in Water Sorption and Proton Conductivity between Nafion and SPEEK. *J. Polym. Sci. Part B Polym. Phys.* **2011**, *49* (20), 1437–1445. https://doi.org/10.1002/polb.22326.

(41) Noureddine, A.; Trens, P.; Toquer, G.; Cattoën, X.; Man, M. W. C. Tailoring the Hydrophilic/Lipophilic Balance of Clickable Mesoporous Organosilicas by the Copper-Catalyzed Azide-Alkyne Cycloaddition Click-Functionalization. *Langmuir* **2014**, *30* (41), 12297–12305. https://doi.org/10.1021/la503151w.

(42) Trens, P.; Denoyel, R.; Guilloteau, E. Evolution of Surface Composition, Porosity, and Surface Area of Glass Fibers in a Moist Atmosphere. *Langmuir* **1996**, *12* (5), 1245–1250. https://doi.org/10.1021/la950531e.

(43) Colomban, P. *Proton Conductors: Solids, Membranes and Gels*, Cambridge.; Cambridge University Press: Cambridge, 1992.

(44) Grotthuss, C. J. . Sur La Décomposition de l'eau et Des Corps Qu'elle Tient En Dissolution à l'aide de l'électricité Galvanique. *Ann. Chim.* **1806**, *58* (54–55).

(45) Nandi, S.; Aggarwal, H.; Wahiduzzaman, M.; Belmabkhout, Y.; Maurin, G.; Eddaoudi, M.; Devautour-Vinot, S. Revisiting the Water Sorption Isotherm of MOF Using Electrical Measurements. *Chem. Commun.* **2019**, *55* (88), 13251–13254. https://doi.org/10.1039/C9CC06012J.

(46) Mileo, P. G. M.; Devautour-Vinot, S.; Mouchaham, G.; Faucher, F.; Guillou, N.; Vimont, A.; Serre, C.; Maurin, G. Proton-Conducting Phenolate-Based Zr Metal-Organic Framework: A Joint Experimental-Modeling Investigation. *J. Phys. Chem. C* **2016**, *120* (43), 24503–24510. https://doi.org/10.1021/acs.jpcc.6b04649.

(47) Mileo, P. G. M.; Kundu, T.; Semino, R.; Benoit, V.; Steunou, N.; Llewellyn, P. L.; Serre, C.; Maurin, G.; Devautour-Vinot, S. Highly Efficient Proton Conduction in a Three-Dimensional Titanium Hydrogen Phosphate. *Chem. Mater.* **2017**, *29* (17), 7263–7271. https://doi.org/10.1021/acs.chemmater.7b01850.

(48) Donnadio, A.; Nocchetti, M.; Costantino, F.; Taddei, M.; Casciola, M.; Da Silva Lisboa, F.; Vivani, R. A Layered Mixed Zirconium Phosphate/Phosphonate with Exposed Carboxylic and Phosphonic Groups: X-Ray Powder Structure and Proton Conductivity Properties. *Inorg. Chem.* **2014**, *53* (24), 13220–13226. https://doi.org/10.1021/ic502473w.

(49) Levenson, D. A.; Zhang, J.; Gelfand, B. S.; Kammampata, S. P.; Thangadurai, V.; Shimizu, G. K. H. Particle Size Dependence of Proton Conduction in a Cationic Lanthanum Phosphonate MOF. *Dalt. Trans.* **2020**, *49* (13), 4022–4029. https://doi.org/10.1039/C9DT04229F.

Table of Contents